PROCEEDINGS A

royalsocietypublishing.org/journal/rspa

Research

Cite this article: Domokos G, Goriely A, Horváth AG, Regős K. 2026 Soft cells, Kelvin foam and the minimal surfaces of Schwarz. *Proc. R. Soc. A* **482**: 20250322. https://doi.org/10.1098/rspa.2025.0322

Received: 16 April 2025
Accepted: 16 March 2026

Subject Areas:
geometry, mathematical modelling, materials science

Keywords:
tessellation, soft cell, Kelvin cell, Dirichlet–Voronoi cell, Schwarz minimal surface

Author for correspondence:
G. Domokos
e-mail: domokos@iit.bme.hu

THE ROYAL SOCIETY
PUBLISHING

Soft cells, Kelvin foam and the minimal surfaces of Schwarz

G. Domokos[1,3], A. Goriely[4], Á. G. Horváth[2,3] and K. Regős[1,3]

[1]Department of Morphology and Geometric Modeling, [2]Department of Algebra and Geometry, and [3]HUN-REN-BME Morphodynamics Research Group, Budapest University of Technology and Economics, Müegyetem rkp 3., Budapest H-1111, Hungary
[4]Mathematical Institute, University of Oxford, Oxford, OX2 6GG, UK

GD, 0000-0002-8676-6829; AG, 0000-0002-6436-8483

We study a class of geometric shapes termed soft cells tiling three-dimensional (3D) space without sharp corners. A special class of soft tilings, called standard soft tilings, can be obtained by an algorithm transforming any convex polyhedral tiling into at least one combinatorially equivalent soft tiling. Natural examples of such shapes include, among others, cell tissues, corals and chambers in nautilus shells. However, this construction leads to sharp, highly curved edges. Here, we generalize this construction to produce not just a single standard soft tiling but all soft tilings corresponding to a given polyhedral configuration. Unlike standard soft cells, these non-standard soft cells do not exhibit protruding edges. Notably, some non-standard soft cells are the fundamental building blocks within triply periodic minimal surfaces (TPMSs) such as Schwarz surfaces and gyroid structures, which are critical in modelling the nanoscale architecture of various polymers and carbon-based materials. These shapes also appear at the nanoscale as fundamental models of biological structures. Finally, we identify a family of intermediate space-filling cells that bridge two distinct soft-cell morphologies, providing a previously unrecognized connection between Schwarz surfaces and encompassing the Kelvin cell, a structure of enduring importance in materials science.

1. Introduction

(a) Motivation

In a recent article [1], we introduced a new class of shapes called *soft cells* that fill space as *soft tilings* without gaps and overlaps while having no sharp corners. We showed that soft cells not only serve as models for chambered seashells, but they can be observed in a broad range of other natural and man-made settings.

Here, we show that the range of applications for soft tilings is even broader than suggested by these early studies. The particular soft-cell shapes illustrated in [1] were obtained by the edge bending (EB) algorithm that restricts the specific geometry of the computed cells. We shall refer to these shapes as *standard* soft cells (see the (f2) and (h2) cells in figure 1).

Here, we introduce the extended EB (EEB) algorithm proving the existence of an entirely new class of *non-standard* soft cells (see the (g2) and (i2) cells in figure 1). Remarkably, these cells are the natural discrete units of triply periodic minimal surfaces (TPMSs), which, in turn, serve as fundamental models in materials science [2–4] and in biology [5–7]. Below we outline the geometric differences between standard and non-standard soft cells and describe the EEB algorithm. The latter not only uncovers the deep connection between soft cells and TPMSs but also reveals one-parameter families of tilings connecting TPMSs to each other in an entirely new manner.

In [1], the EB algorithm served as the main strategy of an *existence proof*, demonstrating that for every element of a broad class of convex tilings there exists at least one combinatorially equivalent soft tiling. The purpose of the EEB is to serve as a possible strategy of a *uniqueness proof*, demonstrating that for a given convex tiling the set of combinatorially equivalent soft tilings can be uniquely determined. In this paper, we demonstrate the feasibility of the EEB algorithm by using it to prove under various symmetry constraints the uniqueness of the set of soft tilings combinatorially equivalent to the tiling by the truncated octahedron. We describe the EEB algorithm in a general fashion that can be applied to other convex tilings, whether it proves to be a successful strategy in other cases remains to be seen. As proof strategies, both the EB and the EEB algorithm rely entirely on analytical techniques and do not use any numerical tools.

(b) Standard and non-standard soft cells

Soft tilings, like polyhedral tilings, have a combinatorial structure defined by the adjacency of vertices, edges and faces. However, it is important to note that edges need not be straight and faces need not be planar. We also define a class of tilings called *polyhedric* that includes, as disjoint subsets, both soft tilings and convex tilings, the latter filling space with convex polyhedra. A key element for the construction of soft tilings is the EB algorithm that preserves the combinatorial structure and the location of vertices and maps a subset of convex tilings (to which we refer as *Hamiltonian* tilings) onto a subset of soft tilings, to which we refer as standard soft tilings and the cells of which we call standard soft cells. Hamiltonian tilings have the property that at every node, the dual of the vertex polyhedron contains a Hamiltonian circuit. Standard soft tilings have the property that at each node, the tangent vector of every incoming edge is collinear.

In this paper, we introduce non-standard soft tilings where the tangent vectors of the edges at nodes are, in general, not collinear. This local feature is dramatically reflected in the difference between the global geometry of standard and non-standard cells: while the former (cells (f2) and (h2) in figure 1) always have razor-sharp, protruding curved edges, the latter (cells (g2) and (i2) in figure 1) do not have this feature. Remarkably, the softness value (defined in [1] for arbitrary, piecewise smooth shapes, see also §5a of the current paper for details) appears to be very high for non-standard soft cells.

Although the EB algorithm guarantees the existence of a standard soft tiling M' that is combinatorially equivalent to a given Hamiltonian tiling M, it does not yield a complete set of

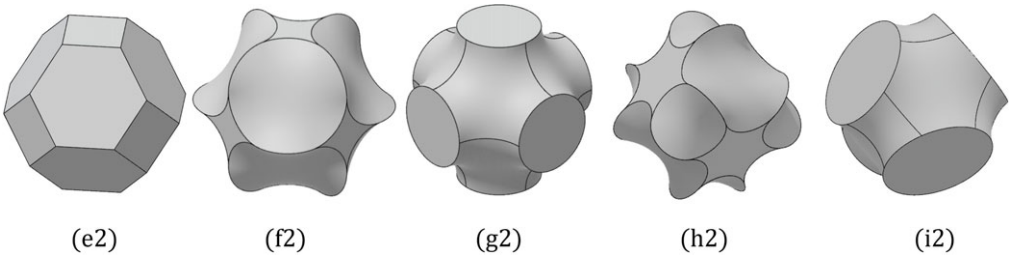

Figure 1. The Dirichlet–Voronoi *bcc* cell (called the (e2) cell in [1]) and its four soft versions. Cells (f2) and (h2) are *standard soft cells* produced by the EB algorithm. Observe protruding curved edges. Cells (g2) and (i2) are *non-standard* soft cells produced by the EEB algorithm. Observe the absence of protruding curved edges.

explicit instructions for the construction of M'. Here, we introduce the EEB algorithm, which, in principle, is capable of proving for any given polyhedral tiling M, the uniqueness of the entire set $\mathcal{M}(M)$ of soft tilings that share the combinatorial structure and vertex locations of M, while satisfying a prescribed symmetry group and other geometric constraints. Depending on the symmetry group and constraints, the set $\mathcal{M}(M)$ may be finite or infinite, and we demonstrate examples for both cases. The two algorithms are closely related: the EB algorithm guarantees that for any given Hamiltonian tiling, the set of combinatorially equivalent soft tilings is non-empty; thus, the uniqueness proof using the the EEB algorithm as the main strategy has a chance to succeed.

(c) Soft cells and triply periodic minimal surfaces

TPMSs are embedded minimal surfaces in $\mathbb{R}^3$ that are invariant under three linearly independent translations, yielding a periodic structure that spans the entire space. The fundamental domains of the translational lattice under which the surface is invariant are unit cells in their own right. Typically, these unit cells are chosen such that the entire surface can be generated by translating the portion within a single cell along three linearly independent lattice vectors. The shape of the unit cell depends on the specific symmetry group of the surface, and the surface within the cell satisfies the minimal surface condition (zero mean curvature) and matches smoothly across opposite faces under the lattice translations. Unit cells are visually not reminiscent of tilings, so, at first sight they are not related to soft cells either. On the other hand, one can construct Voronoi partitions of TPMSs [3,8], which yield soft tilings; we discuss such constructions related to the Schwarz P and Schwarz D surfaces [8,9] in §4. We shall show that the EEB algorithm not only generates the soft tilings associated with these surfaces, but it also helps to identify families of soft tilings connecting them. TPMSs and their unit cells are critical in crystallographic and materials applications, as they define the repeating geometry and influence mechanical and transport properties when such surfaces are used as microstructure templates for materials [3,10]. In fact, there exist allotropes of carbon, called schwarzites [11–13].

Another interesting natural example is the *Kelvin dry foam*. The corresponding cell, known as the *Kelvin cell*, is a space-filling polyhedric cell proposed by Lord Kelvin in 1887 as a solution to the problem of partitioning space into cells of equal volume with minimal surface area [14]. It is based on a truncated octahedron—a convex polyhedron with six square faces and eight regular hexagonal faces. In order to satisfy Plateau's laws for foams, Kelvin's original construction slightly distorts the regular truncated octahedron into a polyhedric shape with curved faces to reduce the total interfacial area while still filling space without gaps. The Kelvin cell approximates the minimal-area solution for discrete equal-volume polyhedric cells in a foam, whereas TPMSs are smooth surfaces with zero mean curvature everywhere.

Here, we describe and use the EEB algorithm to find non-standard soft tilings that are associated with TPMSs, including the Schwarz P and Schwarz D surfaces. The EEB algorithm

generates one-parameter families of solutions, each member of which is a space-filling tiling and the end members of which are soft tilings. Connections between TPMSs have been observed experimentally [15,16]. The connections revealed by the EEB algorithm differ from previously known geometries [17,18] and may serve as the mathematical model of the observed transitions. The one-parameter families produced by the EEB algorithm also connect soft tilings with the geometry of optimal dry foams [14].

(d) Basic notions and the main result

Similarly to the EB algorithm, the output of the EEB algorithm does not fully characterize a soft tiling but only determines both tangent vectors for each edge. The remaining features of the shape defined by the curves carrying edges and the surfaces carrying faces can be determined by additional considerations. Motivated by this common feature of the EB and EEB algorithms, we introduce a classification scheme for polyhedric tilings:

Definition 1.1. Let M be a polyhedric tiling. Then, the zeroth-order description of M is the combinatorial structure of M. The ith-order description ($i = 1, 2, 3, 4$) of M contains the $(i-1)$th-order description and the following additional features:

- $i = 1$: the location of nodes,
- $i = 2$: the unit vectors of edge tangent vectors,
- $i = 3$: the shape of edges, and
- $i = 4$: the shape of faces.

If two tilings M and M' agree up to order k, then we say that they are elements of a kth-order equivalence class of tilings. The ith-order description is characterized by the symmetry group Γ_i with fundamental domain f_i, and we have $\Gamma_i \leq \Gamma_j$ if $i \geq j$.

Definition 1.1 naturally leads to a concise and practical new definition of softness.

Definition 1.2. Let M be a polyhedric tiling with smooth edges and faces. A cell of M is *soft* if each node has at least two unit tangent vectors $\mathbf{u_1}, \mathbf{u_2}$ such that $\mathbf{u_1} \cdot \mathbf{u_2} = -1$. A tiling is *soft* if each cell in the tiling is soft.

Since softness depends on tangent vectors, it is related to the second-order description of the tiling, and it is independent of any higher-order features. As a consequence, both the EB and the EEB algorithms are of second order, operating on tangent vectors, so they do not determine the shape of cells to higher order. If we want to construct a soft tiling explicitly, we need to specify the shape of its edges and faces, which are, respectively, included in the third- and fourth-order descriptions. Therefore, to obtain illustrative examples of second-order soft equivalence classes, we provide the full fourth-order description by imposing that edges are circular arcs with minimal curvature and faces are minimal surfaces.

In this paper, we illustrate the EEB algorithm by using the monohedral Dirichlet–Voronoi tiling on the *bcc* lattice as input. In [1], we called this the (e2) tiling and, using the EB algorithm, developed from (e2) the soft, standard (f2) tiling (figure 1, first two cells from the left-hand side). Using the concepts in definitions 1.1 and 1.2, we can now state our two main results for the (e2) tiling.

Theorem 1.3. *In the first-order equivalence class containing the (e2) tiling there exist exactly two second-order equivalence classes of soft tilings, which share the full symmetry group of (e2). Figure 1 shows the soft cells (f2) and (g2), which, respectively, belong to these two classes.*

Theorem 1.4. *In the first-order equivalence class containing the (e2) tiling there exist exactly four second-order equivalence classes of soft tilings, the cells of which have at least the symmetry group of the regular tetrahedron and have at least one planar face. Figure 1 shows the soft cells (f2), (g2), (h2) and (i2), which, respectively, belong to these four classes.*

Table 1. First-order description of the (e2) cell.

node	x	y	z	node	x	y	z
1	0	0	0	13	2	1	$2/\sqrt{2}$
2	1	0	0	14	1	2	$2/\sqrt{2}$
3	1	1	0	15	0	2	$2/\sqrt{2}$
4	0	1	0	16	−1	1	$2/\sqrt{2}$
5	−1/2	−1/2	$1/\sqrt{2}$	17	−1/2	−1/2	$3/\sqrt{2}$
6	3/2	−1/2	$1/\sqrt{2}$	18	3/2	−1/2	$3/\sqrt{2}$
7	3/2	3/2	$1/\sqrt{2}$	19	3/2	3/2	$3/\sqrt{2}$
8	−1/2	3/2	$1/\sqrt{2}$	20	−1/2	3/2	$3/\sqrt{2}$
9	−1	0	$2/\sqrt{2}$	21	0	0	$4/\sqrt{2}$
10	0	−1	$2/\sqrt{2}$	22	1	0	$4/\sqrt{2}$
11	1	−1	$2/\sqrt{2}$	23	1	1	$4/\sqrt{2}$
12	2	0	$2/\sqrt{2}$	24	0	1	$4/\sqrt{2}$

Table 2. The polyhedral (e2) cell and all four first-order equivalent soft cells with at least tetrahedral symmetry and at least one planar face, given with the $[x, y, z]$ coordinates of the unit vector $\mathbf{a}$ (cf. figure 2) and with Euler angles, where $\theta = 0, \phi = 0$ coincide, respectively, with the x and z axes of the Cartesian system shown in figure 2. Last column: softness value $0 \leq \sigma \leq 1$, as defined in [1].

name	great circles			a_x	a_y	a_z	ϕ	θ	σ
(e2)	g_{hex}	g_{quad}		1	0	0	$\pi/2$	0	0
(f2)	g_{adbc}	g_{quad}	g_{acbd}	$\frac{1}{\sqrt{2}}$	$\frac{1}{\sqrt{2}}$	0	$\pi/2$	$\pi/4$	0.331
(g2)	g_{adbc}	g_{quad}		$\frac{1}{\sqrt{2}}$	$-\frac{1}{\sqrt{2}}$	0	$\pi/2$	$-\frac{\pi}{4}$	0.333
(h2)	g_{adbc}	g_{hex1}	g_{acbd}	$\frac{1}{2}$	$-\frac{1}{2}$	$\frac{1}{\sqrt{2}}$	$\pi/4$	$-\pi/4$	0.464
(i2)	g_{adbc}	g_{hex2}		$\frac{\sqrt{3}}{2}$	$\frac{\sqrt{3}}{6}$	$\frac{1}{\sqrt{6}}$	$\cos^{-1}\frac{1}{\sqrt{6}}$	$\tan^{-1}\frac{1}{3}$	0.474

As we can observe, two of these cells are standard ((f2) and (h2)), the other two ((g2) and (i2)) are non-standard. In §4, we shall prove that the second-order equivalence classes containing (g2) and (i2) also contain, respectively, the unit cells of the Schwarz P and Schwarz D surfaces, serving as models of material microstructure, called *mesoatoms* [3,10].

If we drop the requirement that at least one face should be planar, then the EEB algorithm generates a one-parameter family of soft cells connecting the Schwarz D and Schwarz P unit cells. If we drop the requirement of softness and only require that the quadrangular faces of the (e2) cell remain planar, then the EEB algorithm determines a one-parameter family of space-filling cells that, in addition to the (e2), (f2) and (h2) cells, also includes the *Kelvin cell*, serving as the fundamental model of optimal dry foams [14]. This demonstrates that soft cells are significant not only as final geometric forms but also in terms of their underlying geometric genesis, which may provide valuable insights into modelling structures in natural phenomena.

(e) Structure of the paper

We prove theorems 1.3 and 1.4 in two steps. In §2, we introduce the EEB algorithm. Then, in §3 we give a constructive proof of theorems 1.3 and 1.4 by applying the EEB algorithm to the (e2) tiling and identifying all solutions under the symmetry and geometric constraints stated in

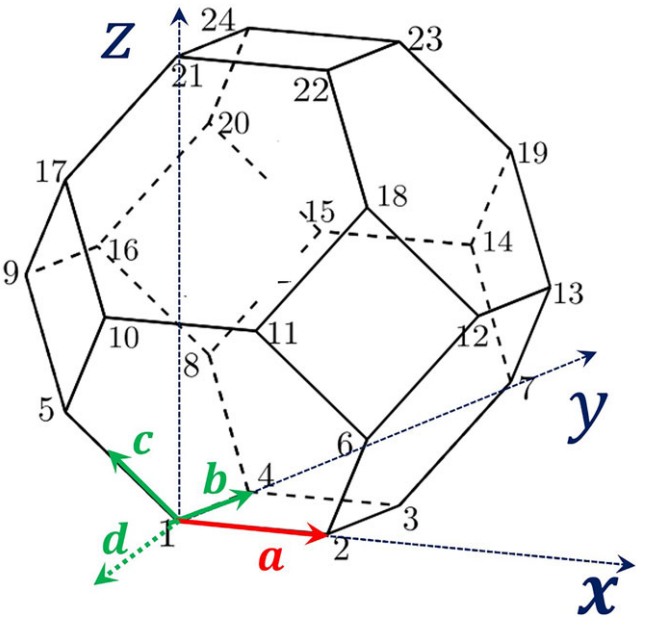

Figure 2. The Dirichlet–Voronoi-*bcc* cell.

the theorems. The list of all solutions in table 2 completes the proof, several essential aspects of which are illustrated in figure 3. After proving theorems 1.3 and 1.4, in §4, we discuss two applications: the Schwarz minimal surfaces and the Kelvin foam. For Schwarz surfaces, we formulate proposition 4.2, claiming that the Schwarz P and D surfaces are well approximated by the (g2) and (i2) tilings, respectively. For the Kelvin cell, we identify explicitly a one-parameter family of space-filling cells which contains the (e2) polyhedral cell, the (f2) and (g2) soft-cells and also the Kelvin cell. Embedding the Kelvin cell into this family not only helps to explain its geometry but also shows that systematically bending the edges of polyhedral tilings may result in physically relevant constructions. In §5, we first discuss open questions. In particular, we describe the soft tiling associated with the gyroid and point out that the related polyhedral tiling is still not fully understood.

(f) Some applications

The observations about the existence of soft cells have been confirmed by other authors: soft-cell shapes have been reported in the context of seashell geometry [19], in cell tissues [20] and corals [21]. Soft cells also emerge naturally in computational elasticity [22] where the presence of sharp corners poses multiple challenges and in finite-element mesh generation algorithms [23]. They have inspired the design of metamaterials [24], and architects have explored the mechanical properties of soft cells when applied as building blocks of masonry structures [25].

2. The extended edge bending algorithm

We only describe the EEB algorithm for monohedric, isogonal tilings M (all cells and all nodes are identical), but all steps can be generalized to the case of multiple cells and nodes.

Definition 2.1. We assume that the polyhedric tiling M is defined to first order, so the symmetry group Γ_1 is known and we also know the symmetry group $\Gamma_2 \leq \Gamma_1$ associated with the second-order description. We assume that at each node N cells and K edges meet, so we have K unit tangent vectors, which we call the *nodal set* of M. From the nodal set, we can construct N different

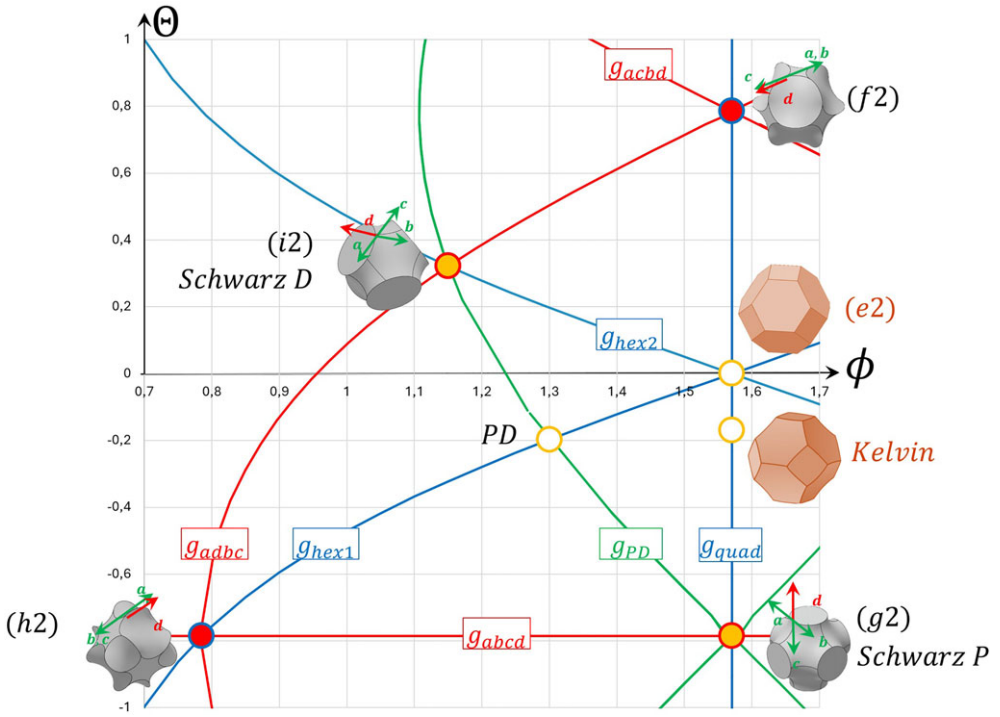

Figure 3. All solutions of the softening equations for the polyhedral (e2) cell shown in figure 2, plotted on the plane (ϕ, θ) of Euler angles ($\theta = 0$, $\phi = 0$ coinciding, respectively, with the *x* and *z* axes of the Cartesian system shown in figure 2). Red lines: great circles solving complete sets of softening equations. Blue lines: great circles solving constraint equations that keep faces planar. Green lines: great circles connect non-standard soft cells. Blue dots with red fill: standard soft cells identified by the intersection of two red lines and one blue line. Red dots with yellow fill: non-standard soft cells defined by the intersection of one blue and one red line. Yellow dots with white fill: non-soft cells. For detailed data on cells (e2), (f2), (g2), (h2) and (i2), see table 2. For data on the Kelvin cell and the *PD* cell, see table 3. For better visibility, nodal set a, b, c, d is shown on vertex 21 instead on vertex 1.

subsets containing tangent vectors, belonging to the N cells. We refer to these sets of vectors as the N *vertex sets* of M, and we denote the size of the vertex sets by v_i, $i = 1, 2, \ldots N$.

Algorithm 2.2. *Using the notions in definition 2.1, the steps of the EEB algorithm are the following:*

(i) *We identify the fundamental domain f_2 of Γ_2 in the second-order description, i.e. we identify a maximal set of unit half tangents $\mathbf{u}_i$, $i = 1, 2, \ldots, f$ which are not related by any transformation of the group Γ_2.*

(ii) *Using the set $\mathbf{u}_i$, $i = 1, 2, \ldots, f$ as inputs, we apply symmetry transformations in Γ_2 to construct the nodal set $\mathbf{u}_i$, $i = 1, 2, \ldots, n$, $n \geq f$ of M.*

(iii) *We pick a pair of half tangents $\mathbf{u}_i, \mathbf{u}_j$ from the nodal set and start writing a list:*

$$\boldsymbol{u}_i \boldsymbol{u}_j = -1. \tag{2.1}$$

We continue picking pairs and add the corresponding equation to the list if the equation does not agree with any previous equation and does not contradict any previous equation. We continue this process until we have at least one equation in every vertex set. At this point, we denote the number of equations by E, and we call this system of equations a complete set of softening equations of M. The same tiling may have several complete sets of softening equations.

(iv) *We let the vectors $\mathbf{u}_i$, $i = 1, 2, \ldots, f$ of the fundamental domain independently run over the boundary of unit sphere. (We may regard the f unit sphere boundaries as a configuration space*

or morphospace [26], containing all possible space-filling cells of the first-order family with given symmetry group.) Since all vectors in the nodal set can be determined via transformation matrices from the fundamental domain, this operation will turn the softening equations into E equations on the sphere in 2f variables and we solve these systems.

(v) If there are additional, prescribed constraints on the geometry of the cells (e.g. planar faces), then we also solve the corresponding equation systems.

(vi) We combine the solutions guaranteeing soft geometry with those guaranteeing additional constraints.

Remark 2.3. We briefly comment on some steps of the algorithm.

— The existence of a solution of any of these systems is a necessary (but not sufficient) condition for the existence of a soft tiling M', which is equivalent to first order to M, has symmetry group Γ_2 and obeys the prescribed additional geometric constraints. Symmetry is not guaranteed since we may have been able to identify the nodal set from the fundamental domain by applying only a subset of Γ_2.

— In general, checking whether two equations are contradictory is far from trivial. However, the set of equations (2.1) is rather special: if we regard them as edges on a graph with n nodes, then cycles of odd length are equivalent to a contradiction.

— Softening equations are often equivalent to eigenvalue problems for the transformation matrices. This is always the case if both unit vectors appearing in the equation have been transformed from the same element of the fundamental set.

3. The (e2) cell and the proof of theorems 1.3 and 1.4

In this section, we discuss the application of the EEB algorithm to the Dirichlet–Voronoi cell on the *bcc* lattice (the (e2) cell), as shown in figure 2 (see also figure 1, left-hand image). Our goal is to prove theorems 1.3 and 1.4. We do the proof in steps numbered as subsections, and the numbering of these subsections corresponds *exactly* to the numbering of the steps in algorithm 2.2. For steps (i), (ii) and (iii), the proofs for both theorems agree. For steps (iv), (v) and (vi), we discuss the two proofs separately. The proofs are concluded after table 2.

Proof. The first-order description of the cell is provided in table 1, defined as the (e2) cell in [1]. While figure 2 shows the polyhedral cell defined to fourth order, we only use the first-order information contained in table 1. ■

(a) Symmetries and the fundamental domain

The *space group* of the (e2) tiling is $\Gamma_1 = Im3m$ (listed as # 229 in [27]), containing the symmetry group of the regular octahedron as a *point group* of order 48. In theorem 1.3, for the second-order description, we require the same symmetry groups. In theorem 1.4, for the second-order description, we require that the soft tiling should have the $\Gamma_2 = Pn3m < \Gamma_1$ space group (listed as # 224 in [27]), containing the symmetry group of the regular tetrahedron as a point group of order 24. In both cases (theorems 1.3 and 1.4), the fundamental domain f_2 of the second-order description is a single unit vector (i.e. we have $f = 1$) and we pick $\mathbf{a}$ (in the polyhedral tiling $\mathbf{a} = (1, 0, 0)^T$). So we have $\mathbf{u}_1 \equiv \mathbf{a}$.

The nodal set of this tiling consists of four vectors (so we have $n = 4$), which we show in figure 2 at vertex 1, denoted by $\mathbf{a}, \mathbf{b}, \mathbf{c}, \mathbf{d}$, respectively, so we have $\mathbf{u}_2 \equiv \mathbf{b}, \mathbf{u}_3 \equiv \mathbf{c}, \mathbf{u}_4 \equiv \mathbf{d}$. These vectors can be obtained from the vector $\mathbf{a}$ via the following linear transformations:

$$\mathbf{b} = T_b\mathbf{a}, \quad \mathbf{c} = T_c\mathbf{a} \quad \text{and} \quad \mathbf{d} = T_{d,i}\mathbf{a}, \quad (i = 1, 2), \tag{3.1}$$

where

$$T_b = \begin{pmatrix} 0 & 1 & 0 \\ 1 & 0 & 0 \\ 0 & 0 & -1 \end{pmatrix} \quad \text{and} \quad T_c = \begin{pmatrix} -\frac{1}{2} & -\frac{1}{2} & \frac{1}{\sqrt{2}} \\ -\frac{1}{2} & -\frac{1}{2} & -\frac{1}{\sqrt{2}} \\ \frac{1}{\sqrt{2}} & -\frac{1}{\sqrt{2}} & 0 \end{pmatrix} \tag{3.2}$$

and

$$T_{d,1} = \begin{pmatrix} -\frac{1}{2} & -\frac{1}{2} & +\frac{1}{\sqrt{2}} \\ -\frac{1}{2} & -\frac{1}{2} & -\frac{1}{\sqrt{2}} \\ -\frac{1}{\sqrt{2}} & +\frac{1}{\sqrt{2}} & 0 \end{pmatrix} \quad \text{and} \quad T_{d,2} = \begin{pmatrix} -\frac{1}{2} & -\frac{1}{2} & -\frac{1}{\sqrt{2}} \\ -\frac{1}{2} & -\frac{1}{2} & +\frac{1}{\sqrt{2}} \\ -\frac{1}{\sqrt{2}} & +\frac{1}{\sqrt{2}} & 0 \end{pmatrix}. \tag{3.3}$$

The transformations T_b, T_c apply for both symmetry groups (and thus both theorems). The transformation producing the vector $\mathbf{d}$ is different in the two cases, $T_{d,1}$ applies for octahedral symmetry, in the proof of theorem 1.3 and $T_{d,2}$ applies for tetrahedral symmetry, in the proof of theorem 1.4.

(b) Nodal set and vertex sets

Since we are dealing with a primitive Voronoi tiling, four cells meet at a node so we have $N = 4$. For the same reason, the size of all vertex sets is equal, and we have $v_i = 3$, $i = 1, 2, 3, 4$. The vectors $(\mathbf{a}, \mathbf{b}, \mathbf{c})$ compose the vertex set of the cell visible in the figure. There are three other cells meeting at this vertex, and their respective vertex sets are $(\mathbf{a}, \mathbf{b}, \mathbf{d})$, $(\mathbf{a}, \mathbf{c}, \mathbf{d})$ and $(\mathbf{b}, \mathbf{c}, \mathbf{d})$.

(c) Complete sets of softening equations

For this system, we can write three different complete sets of softening equations:

$$\mathbf{ab} = -1, \quad \mathbf{cd} = -1, \tag{3.4}$$

$$\mathbf{ac} = -1, \quad \mathbf{bd} = -1 \tag{3.5}$$

and

$$\mathbf{bc} = -1, \quad \mathbf{ad} = -1. \tag{3.6}$$

(d) Solution of the softening equations

Now we make step (iv) of the algorithm and let the fundamental domain of the second-order description (the unit vector $\mathbf{a}$) run over the sphere.

(i) Octahedral symmetry: solutions of the equations in the proof of theorem 1.3

First we solve system (3.4). The first equation yields the great circle g_{ab} with unit normal

$$\mathbf{u}_{ab} = \left(\frac{1}{\sqrt{2}}, \frac{1}{\sqrt{2}}, 0\right)^T, \tag{3.7}$$

while the second equation has an isolated solution at

$$\mathbf{a}_{cd} = \left(\frac{1}{\sqrt{2}}, -\frac{1}{\sqrt{2}}, 0\right)^T. \tag{3.8}$$

Next, we solve system (3.5). The first equation yields the great circle g_{ac} with unit normal

$$\mathbf{u}_{ac} = \left(\frac{1}{2}, -\frac{1}{2}, \frac{1}{\sqrt{2}}\right)^T, \tag{3.9}$$

while the second equation has an isolated solution at

$$\mathbf{a}_{bd} = \left(\frac{1}{\sqrt{2}}, \frac{1}{\sqrt{2}}, 0\right)^T. \tag{3.10}$$

Next, we solve system (3.6). The first equation yields the great circle g_{bc} with unit normal

$$\mathbf{u}_{bc} = \left(-\frac{1}{2}, \frac{1}{2}, \frac{1}{\sqrt{2}}\right)^T, \tag{3.11}$$

while the second equation has an isolated solution at

$$\mathbf{a}_{ad} = \mathbf{a}_{bd} = \left(\frac{1}{\sqrt{2}}, \frac{1}{\sqrt{2}}, 0\right)^T. \tag{3.12}$$

(ii) Tetrahedral symmetry: solutions of the equations in the proof of theorem 1.4

If we solve the three equation systems (3.4)–(3.6) for the unit vector $\mathbf{a}$, the solutions are great circles that are denoted, respectively, by $g_{abcd} \equiv g_{ab}, g_{acbd} \equiv g_{ac}$ and $g_{adbc} \equiv g_{bc}$, the respective unit normals given in equations (3.7), (3.9) and (3.11). We can observe that g_{acbd} and g_{adbc} are related by symmetry with respect to the diagonal plane $x = y$, so henceforth we only identify solutions related to the former.

(e) Additional constraints: planar faces

In theorem 1.3, there are no additional constraints; however, in theorem 1.4, we added the constraint that at least one face should remain planar, so this subsection is related only to the proof of theorem 1.4. For planar face constraints, it follows that if a great circle solves the problem, then it must lie in the plane of the given face. We solve the corresponding constraint equations to ensure that such a solution actually exists.

The condition that the quadrangular face $(1, 2, 3, 4)$ should remain planar can be written as

$$\mathbf{u}_{\text{quad}}\mathbf{a} = 0 \quad \text{and} \quad \mathbf{u}_{\text{quad}}\mathbf{b} = 0, \tag{3.13}$$

where $\mathbf{u}_{\text{quad}} = (0, 0, 1)^T$ is the unit normal of the quadrangular face. The solution of the system (3.13) is the great circle g_{quad} with unit normal $\mathbf{u}_{\text{quad}}$.

The condition that the hexagonal face $(1, 2, 6, 10, 11, 5)$ should remain planar can be written as

$$\mathbf{u}_{\text{hex1}}\mathbf{a} = 0 \quad \text{and} \quad \mathbf{u}_{\text{hex1}}\mathbf{c} = 0, \tag{3.14}$$

where $\mathbf{u}_{\text{hex1}} = (0, 2/\sqrt{6}, \sqrt{2}/\sqrt{6})^T$ represents the unit normals of the hexagonal face. An analogous condition for face $(1, 4, 8, 16, 9, 5)$ yields $\mathbf{u}_{\text{hex2}} = (2/\sqrt{6}, 0, \sqrt{2}/\sqrt{6})^T$. These solutions correspond to the great circles $g_{\text{hex1}}, g_{\text{hex2}}$ with respective unit normals $\mathbf{u}_{\text{hex1}}, \mathbf{u}_{\text{hex2}}$.

(f) Combining solutions: isolated cells

Now we can conclude the proofs of theorems 1.3 and 1.4, and we discuss these separately.

(i) Octahedral symmetry: completing the proof of theorem 1.3

As we can observe, all equation systems yield one great circle and one isolated point on that great circle. This would provide three isolated solutions; however, the solutions of the systems (3.5) and (3.6) are identical, so we obtain two isolated solutions, given in equations (3.8) and (3.10), corresponding to the soft cells (f2) and (g2), respectively, listed in table 2. Figure 3 illustrates, among others, these two soft cells along with the great circles g_{abcd}, g_{acbd} on the plane (ϕ, θ) of the Euler angles.

(ii) Tetrahedral symmetry: completing the proof of theorem 1.4

We observe that all equation systems yield a one-parameter family of solutions, each family being equivalent to a great circle on the unit sphere. To obtain *isolated* solutions we regard suitable *pairs* of these great circles. We pick pairs in such a manner that for each pair one great circle should guarantee the softness, the other should guarantee at least one planar face. We also consider that

the great circles g_{acbd} and g_{adbc} are related by the $x \leftrightarrow y$ reflection symmetry, so it is sufficient to consider one of them to obtain all solutions that are not related by a symmetry transformation. Using these considerations, we obtained the four soft solutions (f2), (g2), (h2) and (i2), as listed in table 2. The polyhedral cell (e2) is listed in the first row of the table, as it can be obtained by combining the solutions for planar hexagonal and planar quadrangular faces. In the table, we not only identify the great circles the intersection of which determine the given cell but also give the Cartesian coordinates and the corresponding Euler angles for the unit vector a. From the latter, the entire tiling can be reconstructed to second order by the action of the space group $\Gamma_2 = Pn3m$.

Figure 3 illustrates both the four soft cells satisfying all constraints but also the polyhedral cell ($e2$) and the great circles $g_{abcd}, g_{acbd}, g_{\mathrm{hex1}}, g_{\mathrm{hex2}}$ and g_{quad} on the plane (ϕ, θ) of the Euler angles.

We note that the listed solutions are only defined to second order, i.e. each soft cell that appears as an isolated point on the plane of Euler angles represents an infinite set of soft cells with identical vertex locations and identical tangent vectors for the edges. The cells appearing in figures 1 and 3 are particular elements of this infinite set. We picked these elements by using circular arcs as edges and minimal surfaces as faces.

4. Applications

(a) Schwarz minimal surfaces

As previously introduced, TPMSs are smooth, continuous, minimal surfaces (i.e. with zero mean curvature) characterized by three independent, periodic directions in three-dimensional (3D) space. Beyond their unique geometrical role [28], they are highly relevant as models in material science [3,10–12]. While the primary geometric interpretation of a TPMS is that of an *interface*, the same object can also be interpreted as a *tiling*. This interpretation is certainly not new. While many aspects have been described both from the geometrical [8] and physical [3] perspective, we are not aware of a clear definition connecting TPMSs to tilings. Hence, our first goal is to define this connection.

TPMSs generate a special binary partition of 3D space: each partition is a *labyrinth* formed by a tubular system with infinitely many branching points [8]. Hence, a given TPMS gives rise to two tubular labyrinths with branching points. Both tubular labyrinths can be collapsed onto a respective *skeletal graph* and the nodes of which correspond to branching points (see figure 4, panels (a1),(b1)), so TPMSs are associated to a pair of infinite skeletal graphs. Since TPMSs are smooth, so the cross section of the tubes is also a smooth curve. This implies a simple observation:

Observation 4.1. The Voronoi partition of a TPMS labyrinth with respect to the nodes of its skeletal graph results in a soft tiling. We call the cell of this tiling the Voronoi cell associated with the TPMS. If the two labyrinths are identical and the skeletal graph has identical edges and vertices, then this tiling is monohedric and the Voronoi cell of the tiling is a monohedric soft cell. Monohedric Voronoi tilings have been used as physical models of materials structure, and they were called *mesoatoms* [3].

The first TPMS was identified by Riemann [29] and independently by Schwarz [9] who also found another example; these two surfaces are dubbed as the Schwarz D ('diamond') and the Schwarz P ('primitive') surface, respectively. Panels (a1) and (b1) of figure 4 show a Voronoi cell of these surfaces along with a portion of their skeletal graphs. For both the Schwarz P and the Schwarz D surface, the dual labyrinth is identical to the one shown in the figure, and the skeletal graphs are isogonal, i.e. their nodes are identical. The degree n of their nodes is characteristic of the symmetry of their Voronoi cells, as it defines the number of neighbour cells in the same labyrinth. In the case of the Schwarz P surface, we have a node of degree $n = 6$ with cubic symmetry, and in the case of the Schwarz D surface, we have $n = 4$ with tetrahedral symmetry. Remarkably, these surfaces are related to the soft tilings we demonstrated in §2:

Proposition 4.2. *The Voronoi cells of the Schwarz P and Schwarz D minimal surfaces are equivalent to second order to the soft cells (g2) and (i2), respectively.*

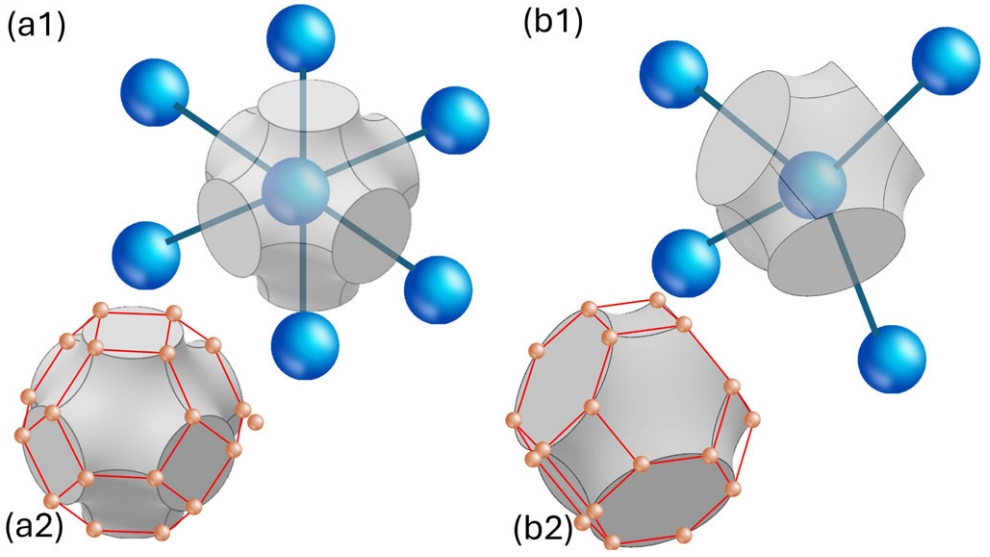

Figure 4. Discrete structures on TPMSs. Upper row, (a1)–(b1): unit cells and skeletal graphs. Bottom row, (a2)–(b2): unit cells carrying the vertices of the skew polyhedron $\{6|4,4\}$. Left column, (a1)–(a2): Schwarz P surface. Right column, (b1)–(b2): Schwarz D surface.

Proof. Here, we regard the soft tilings defined by two TPMSs: the Schwarz P and Schwarz D surfaces, as illustrated in figure 4. According to Schoen [8], the unit cell of the Schwarz P surface has octahedral symmetry (see also [30]) and the unit cell of the Schwarz D surface has tetrahedral symmetry, and both are equivalent to the (e2) tiling to first order: they carry the vertices of the regular map $\{6,4|4\}$ [31], which is, to third order, composed of the truncated octahedra (see panels (a2) and (b2) of figure 4). Based on observation 4.1, we also know that both Schwarz Voronoi cells have n smooth, planar faces. According to theorem 1.4, there are four soft tilings that are first-order equivalents of the (e2) tiling and also carry planar faces. Two of these tilings have a unit cell where the planar faces are non-smooth: these are the standard soft cells (f2) and (h2). The only remaining two cells are (g2) and (i2), so the two Schwarz cells have to be equivalent to these cells to second order. ■

(b) The Kelvin cell

A notable, historic example for curved tilings is the geometric model of dry foams where the tiling has to obey Plateau's Laws [32]. While the structure of foams is strongly reminiscent of polyhedral tilings, there is no space-filling polyhedron meeting this requirement. William Thomson (Lord Kelvin), when faced with this dilemma, proposed to *slightly modify* the truncated octahedron by deforming its edges [14]. The result is a monohedric tiling that became known as the *Kelvin foam* and its cell as the *Kelvin cell* (see figure 5), which has also been investigated for its mechanical properties [33]. While the Weaire–Phelan structure corresponds to a lower energy [34], the Kelvin cell is, to this date, believed to have the smallest surface area among solids that tile space as monohedric cells [34–36].

The Kelvin foam is identical to the (e2) tiling (see figure 2) to first order and it is invariant under the $\Gamma_1 = Im3m$ space group. Similarly to the previously discussed soft cells, the fundamental domain is represented by the vector $\mathbf{a}$. Below we determine the coordinates of $\mathbf{a}$, both in the Cartesian (x,y,z) system as well in Euler angles.

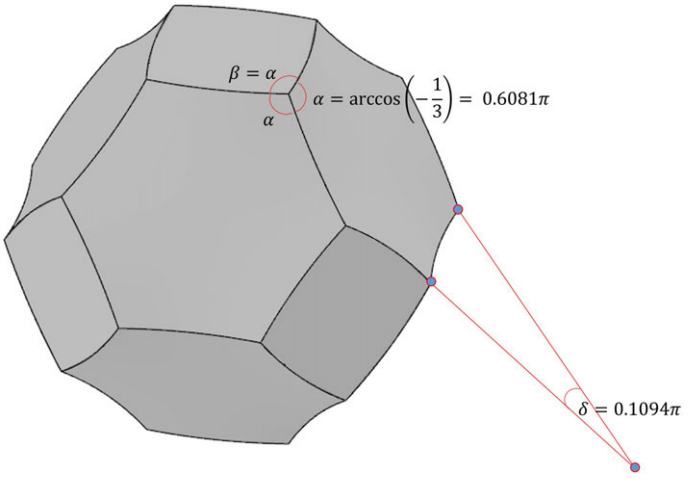

Figure 5. The Kelvin cell.

Table 3. The Kelvin cell and the *PD* cell. See figure 3 for the representation on the plane of the Euler angles.

name	great circles	a_x	a_y	a_z	ϕ	θ
Kelvin	g_{quad}	$1/\sqrt{1+(2\sqrt{2}-3)^2}$	$(2\sqrt{2}-3)/\sqrt{1+(2\sqrt{2}-3)^2}$	0	$\pi/2$	$\tan^{-1}(2\sqrt{2}-3)$
PD	g_{PD} g_{hex1}	$\frac{5}{\sqrt{28}}$	$\frac{-1}{\sqrt{28}}$	$\frac{\sqrt{2}}{\sqrt{28}}$	$\cos^{-1}(\frac{1}{\sqrt{14}})$	$\tan^{-1}(-\frac{1}{5})$

The geometric constraint equations defining the Kelvin cell to second order describe Plateau's law for the edges, prescribing that all edges meet at identical angles, yielding

$$\mathbf{ab} = \mathbf{ac} = \mathbf{ad} = \mathbf{bc} = \mathbf{bd} = \mathbf{cd}. \tag{4.1}$$

We find that from system (4.1), the equation $\mathbf{ac} = \mathbf{ad}$ yields

$$a_z = 0. \tag{4.2}$$

Also, from system (4.1), it follows that the four vectors point to the vertices of a regular tetrahedron, yielding

$$\mathbf{ab} = \mathbf{ac} = \mathbf{ad} = \mathbf{bc} = \mathbf{bd} = \mathbf{cd} = -\frac{1}{3}. \tag{4.3}$$

If we pick $\mathbf{ab} = -1/3$ from equation (4.3) and we substitute equation (4.2) into this equation, we get the solution listed in table 3. This also satisfies system (3.13), the Kelvin cell has $Im3m$ space symmetry and the tiling is invariant under the $z \to -z$ reflection, implying that the quadrangular faces of the cell are planar.

We observe that the g_{quad} great circle contains a one-parameter family of space-filling cells that are first-order equivalents of the (e2) cell and that connect the latter with the (f2) standard soft cell and the Kelvin cell. The morphological evolution corresponding to the g_{quad} great circle has also been observed in computer simulations related to carbon allotropes called schwarzites (cf. fig. 5 in [13]). We also note that there exist other schwarzites that are combinatorially equivalent to the Schwarz D surface, so its Voronoi cells are discrete versions of the (i2) cell [11].

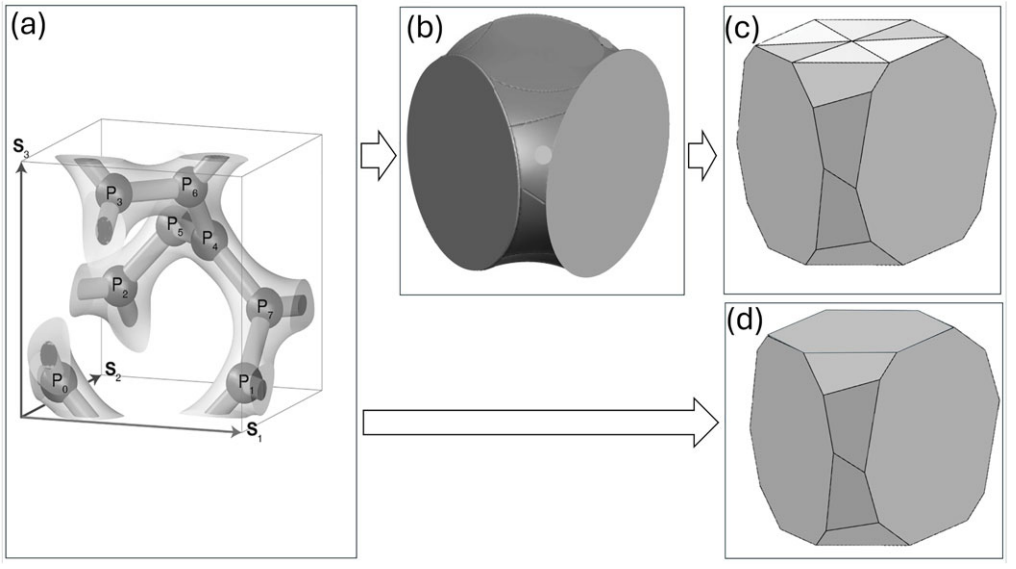

Figure 6. The gyroid cell. (a) One labyrinth of the gyroid with $n = 3$ order nodes P_i, $i = 0, 1, 2, 3, 4, 5, 6, 7$ (see [11], fig. 1e). (b) Soft, space-filling G cell, obtained by Voronoi decomposition of the gyroid labyrinth [3]. (c) Non-convex, space-filling monohedral cell obtained by first-order approximation of the G cell. (d) Convex, space-filling monohedral cell L_2V_{17}, obtained by Voronoi decomposition of 3D space using the nodes P_i [8].

5. Open questions and summary

(a) The gyroid cell

The Schwarz P and D surfaces are related by the continuous bending transformation described in 1853 by Ossian Bonnet [17]. They are members of a one-parameter family of surfaces, called the Bonnet family, with free parameter α, at values $\alpha = 0$ (D) and $\alpha = \pi/2$ (P). Beyond the Schwarz P and D surfaces, there is one single member of this family (at $\alpha \approx 0.663225$), which has no self-intersections: this TPMS, discovered by Alan Schoen [8], is called the gyroid.

While the gyroid is included in the same Bonnet family as the Schwarz P and D surfaces, its geometry is radically different. While the gyroid also gives rise to two identical labyrinths (differing only in handedness), the nodes of the skeletal graphs are of degree $n = 3$, and in a unit cube, there are eight such nodes (see panel (a) of figure 6, based on fig. 1e in [11]). According to Schoen [8], the space group of the gyroid surface is the $I4_132$ group (# 214 in the list provided in [27]).

Panel (a) of figure 6 shows the qualitative picture of one labyrinth of the gyroid. Using observation 4.1, one can obtain the soft, monohedric G cell in panel (b). In [1], we defined a softness value $0 \leq \sigma \leq 1$ for solids S in the following manner: let P_S be a point on the boundary of S. Then, the rolling radius $\rho(P_S)$ of S at P_S is defined as the supremum of the rolling radii of any planar section of S at P_S. We call the infimum of rolling radii of all points P_S on the boundary of S the rolling radius $\rho(S)$ of S. We define the softness of S as $\sigma(S) = \rho(S)\sqrt{2\pi/A(S)}$, where $A(S)$ is the surface area of S. If S is at least C^2-smooth, then $\rho(S)$ is the infimum of radii corresponding to the smaller principal curvature and $\rho(S) = 0$ as soon as S has a sharp corner. As we can see, $\sigma = 0$ for shapes with sharp corners, and we have $\sigma = 1$ on the circular disc. We computed the softness value σ for this cell and found $\sigma = 0.576$, which is the highest value computed so far for any monohedric soft cell. Subsequently, by removing all edges and all faces, we took the first-order approximation of this soft cell and obtained the *non-convex*, space-filling polyhedron, as shown in panel (c). (Recall, that in the case of the Schwarz P and Schwarz D surfaces this operation

results in the convex (e2) cell.) In the next step, we used the nodes P_i of the labyrinth to construct the Voronoi tiling of 3D space, resulting in the convex polyhedron shown in panel (d). Although the difference between the polyhedra in panels (c) and (d) is small, it remains clearly noticeable. Importantly, the same procedure of constructing a Voronoi tiling of space with respect to the nodes of the labyrinth yields, for both Schwarz surfaces, the (e2) cell, which precisely matches the polyhedral approximation of the soft Voronoi cells.

Schoen [8] noticed this peculiar property for the gyroid, and he found the convex polyhedron in panel (d), identified it as the L_2V_{17} polyhedron and called the corresponding monohedral tiling a *toy model* of the gyroid. Apparently, Schoen was aware of the difference between the polyhedra in panels (c) and (d) of figure 6, and he also commented that the gyroid is not associated directly with any convex tiling.

In principle, the EEB algorithm can be applied to prove the existence and uniqueness of the set of all soft cells that are first-order equivalents of a given polyhedral tiling. However, in the case of the non-convex polyhedron shown in panel (c), this proof appears to be particularly challenging. Nonetheless, determining whether another soft cell exists that is first-order equivalent to the soft gyroid cell is an intriguing open question, given the significant role the gyroid structure plays in characterizing material microstructures [3,12].

(b) Connecting the Schwarz surfaces

As noted earlier, the Schwarz surfaces P and D represent the endpoints of a one-parameter family of minimal surfaces originally described by Bonnet [17]. Such one-parameter families, in which one soft cell continuously transforms into another, are more than important mathematical objects as they have also been observed experimentally [15,16], highlighting their practical relevance in physical systems. The geometry of such transitions has also been investigated mathematically [18]. The interpretation of both Schwarz surfaces as soft tilings (g2) and (i2) admits additional one-parameter connections between them, which differ from the one-parameter families given in [17] and [18]. We describe these connections below.

Both (g2) and (i2) are first-order equivalents of the (e2) tiling satisfying two additional constraints: both result from the Voronoi decomposition of tubular labyrinths and both are soft tilings. If we relax either the first or the second of the latter two properties, then we find one-parameter families of first-order (e2) tilings that connect the Schwarz P to the Schwarz D surface.

First, we relax the Voronoi construction: this is equivalent to relaxing the constraint of planar faces. This results in the connection (g2) → (h2) → (i2), consisting entirely of *soft tilings*. This connection, along the great circles g_{abcd} and g_{adbc}, is marked by red lines in figure 3. Next, we relax the softness condition and keep the constraint of planar faces. This results in the connection (g2) → (e2) → (i2), consisting entirely of suitably defined *Voronoi tilings*. This connection, along the great circles g_{quad} and g_{hex2}, is marked by blue lines in figure 3. We may also relax *both* conditions. In this case, any one-parameter curve on the unit sphere passing through (g2) and (i2) may be chosen. The shortest path is the great circle g_{PD}, marked by the green line in figure 3, connecting the soft cells (g2) and (i2). We determined the unit normal as

$$\mathbf{u}_{PD} = \left(\frac{1}{\sqrt{12}}, \frac{1}{\sqrt{12}}, -\frac{2}{\sqrt{6}}\right). \tag{5.1}$$

While this solution appears to provide the most natural link between first-order (e2) tilings, it remains unclear what specific geometric constraint it imposes on the shape of the corresponding cell. If we consider the intersection of the solutions g_{PD} and g_{hex1}, we obtain an isolated solution, which we refer to as the *PD cell*. The coordinates of this cell are listed in table 3. Notably, the PD cell is not soft; the relevant scalar products can be explicitly calculated as $\mathbf{ab} = -3/7$, $\mathbf{ac} = 1/7$ and $\mathbf{bc} = -5/7$.

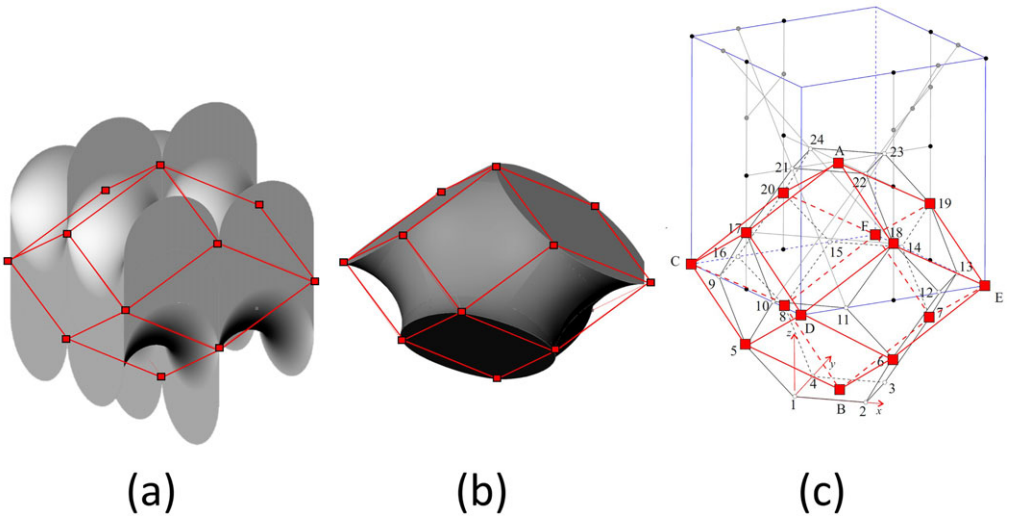

Figure 7. Soft cells in the first-order equivalence class of the rhombododecahedron. (a) The (f3) soft cell demonstrated in [1], obtained by the EB algorithm from the rhombododecahedron. (b) The (g3) soft cell that is a natural unit cell of the Schwarz D surface. (c) Structure drawing showing the relationship of the truncated ocathedron and the rhombododecahedron as discrete structures carried by the Schwarz D surface.

(c) Soft tilings and symmetry groups

Observation 4.1 identified the soft cells generated by Voronoi partitions of TPMSs, and in proposition 4.2, we were able to identify the Voronoi cell of the Schwarz P and Schwarz D surfaces with the soft cells (g2) and (i2), both being first-order equivalent to the truncated octahedron (e2) cell. The soft tilings associated with these cells exhibit the full symmetry of their corresponding minimal surfaces, as their vertices align precisely with those of the regular map $\{6, 4|4\}$ described by Coxeter [31]. Furthermore, TPMSs accommodate various other regular maps and infinite polyhedra, each defining distinct soft monohedric tilings with reduced symmetry groups. These discrete structures thus enable the generation of soft monohedric tilings characterized by a range of smaller symmetry groups.

As an illustration, in addition to the (i2) cell (shown in figures 1 and 3) in figure 7b, we show another soft cell associated with the Schwarz D surface. The (i2) cell was derived by the EEB algorithm, via softening the Voronoi cell of the *bcc* lattice (shown in figure 2). However, the Schwarz D surface also carries the nodes of the monohedral tiling by the rhombododecahedron that is the Brillouin zone of the *bcc* lattice and the Voronoi cell of the dual *fcc* lattice, and we used this alternative tiling to obtain another soft unit cell. Whether or not the rhombododecahedral cell has other first-order equivalent soft versions is an intriguing open question that could be addressed by the EEB algorithm and may offer new insight into the geometry of the Schwarz surfaces.

We also remark that, according to theorem 1.3, the soft tilings (f2) and (g2) inherit the full symmetry group of the (e2) polyhedral tiling, the latter being one of the five Dirichlet–Voronoi cells of point lattices [37,38]. An examination of the remaining four Dirichlet–Voronoi cells shows that no corresponding soft tiling exists that preserves the full symmetry group of their polyhedral mosaics. An intriguing open question is whether, aside from the (f2) and (g2) tilings, there exist additional soft tilings that fully inherit the symmetry of their respective polyhedral tilings.

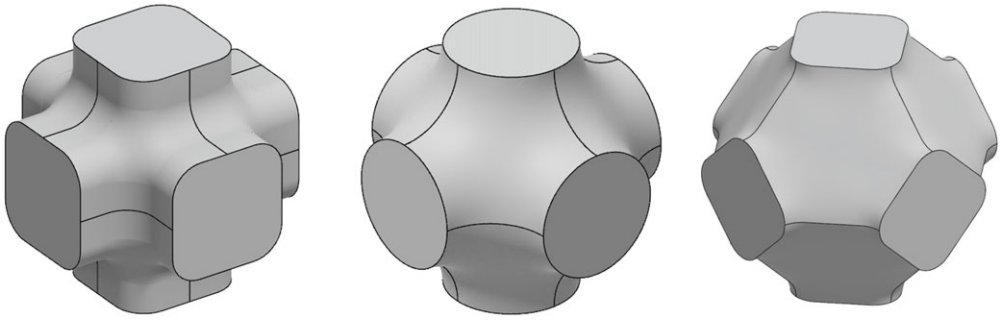

Figure 8. Three members of the second-order family (g2) of soft cells, containing also the Schwarz P unit cell.

(d) Second-order families of soft cells

Although we only used its second-order structure, the (e2) cell in figure 1 is determined to fourth order and the same holds for the Kelvin cell in figure 5. In contrast, the four soft cells (f2), (g2), (h2) and (i2) appearing in theorem 1.4 and later in our computations are, strictly speaking, only determined to second order. The images shown in figures 1 and 3 are examples of these second-order families where we complemented the second-order structure by circular edges and minimal surfaces as faces, to obtain the full geometry of the cells. Indeed, the proof of proposition 4.2 relies precisely on the insight that specifying the exact geometric form of the Schwarz P and D cells is unnecessary to identify them as members of the (g2) and (i2) families. Visually, however, the differences between the Schwarz cells and the illustrated examples of the (g2) and (i2) families are minimal. To emphasize that our analysis is limited to second-order considerations and thus does not entirely constrain the cell shapes, we provide two additional examples of cells belonging to the (g2) family in figure 8.

(e) Concluding remarks and questions

In this paper, we introduced and described the EEB algorithm, which offers a strategy to prove the uniqueness of the set containing *all* soft cells sharing the vertices of a given polyhedral tiling. To demonstrate the effectiveness of this algorithm, we applied it to the Dirichlet–Voronoi tiling of the *bcc* lattice. We proved that exactly two types of soft cells exist, determined up to the tangent vectors of their edges, which share the vertices and the full symmetry group of the polyhedral tiling. We also proved that exactly four types of soft cells exist, determined up to the tangent vectors of their edges, that share the vertices of this monohedral tiling, exhibit at least tetrahedral symmetry and possess at least one planar face. Furthermore, we established that two of these soft cells correspond precisely to the Voronoi cells associated with the Schwarz P and Schwarz D minimal surfaces, respectively.

We remark that theorems 1.3 and 1.4 state that the EEB algorithm can be applied to the (e2) tiling, and they explicitly describe the results of this application, i.e. the output of the EEB algorithm with the (e2) tiling as an input. While the EEB algorithm could *in principle* be applied to any polyhedral tiling, as the number of polyhedra and the number of edges meeting at a node increase and also the number of node types increases, the application of the EEB algorithm becomes increasingly challenging from a practical perspective.

Since this paper connects non-standard soft tilings to standard soft tilings, it is natural to ask where the latter may appear in material structure and what would be the mechanical properties of lattice materials with the geometry of standard soft tilings. One early indication is an architectural experiment [25] where the authors used standard soft cells as masonry blocks and found that the mechanical behaviour of the resulting structure was better than that of conventional brick masonry. There is also some indication that standard soft tilings are linked to cell membranes

[20]. More connections will help us to understand the underlying growth mechanisms and the mechanical properties of these structures.

Soft cells and soft tilings appear as a geometric concept linking a broad variety of natural phenomena. The EEB algorithm has successfully expanded the domain of known soft cells and identified soft cells that differ fundamentally from the standard examples previously illustrated in [1]. This discovery significantly expands the spectrum of potential applications and invites exciting new explorations into the diversity of soft-cell geometries yet to be uncovered.

Data accessibility. This article has no additional data.

Declaration of AI use. We have not used AI-assisted technologies in creating this article.

Authors' contributions. G.D.: conceptualization, formal analysis, investigation, methodology, supervision, writing—original draft, and writing—review and editing; A.G.: investigation, methodology, writing—original draft and writing—review and editing; Á.G.H.: formal analysis, investigation, methodology, writing—original draft and writing—review and editing; K.R.: investigation, methodology, visualization, and writing—review and editing.

All authors gave final approval for publication and agreed to be held accountable for the work performed therein.

Conflict of interest declaration. We declare we have no competing interests.

Funding. This research was supported by NKFIH grant no. K149429 and EMMI FIKP grant VIZ (K.R. and G.D.). This research has been supported by the program UNKP-24-3 funded by ITM and NKFI (K.R.). The research was also supported by the Doctoral Excellence Fellowship Programme (DCEP) funded by ITM and NKFI and the Budapest University of Technology and Economics.

Acknowledgements. The authors sincerely thank Greg Grason for the stimulating, in-depth discussion on the geometry of mesoatoms and for pointing out the ongoing experimental work on transitions between Schwarz surfaces. The authors also thank three anonymous referees for stimulating comments and suggestions. The authors also thank an anonymous referee for suggesting the investigation of lower symmetries that led to the discovery of the (g3) cell. The gift representing the Albrecht Science Fellowship is gratefully appreciated.

References

1. Domokos G, Goriely A. 2024 Soft cells and the geometry of seashells. *PNAS Nexus* **3**, pgae311. (doi:10.1093/pnasnexus/pgae311)
2. Chen Z, Xie YM, Wu X, Wang Z, Li Q, Zhou S. 2019 On hybrid cellular materials based on triply periodic minimal surfaces with extreme mechanical properties. *Mater. Des.* **183**, 108109. (doi:10.1016/j.matdes.2019.108109)
3. Grason GM, Thomas EL. 2023 How does your gyroid grow? A mesoatomic perspective on supramolecular, soft matter network crystals. *Phys. Rev. Mater.* **7**, 045603. (doi:10.1103/PhysRevMaterials.7.045603)
4. Jones A, Leary M, Bateman S, Easton M. 2022 Parametric design and evaluation of TPMS-like cellular solids. *Mater. Des.* **221**, 110908. (doi:10.1016/j.matdes.2022.110908)
5. Breish F, Hamm C, Kienzler R. 2025 Beyond global mechanical properties: bioinspired triply-periodic minimal surface cellular solids for efficient mechanical design and optimization. *Adv. Eng. Mater.* **27**, 2402105. (doi:10.1002/adem.202402105)
6. Wilts BD, Zubiri BA, Klatt MA, Butz B, Fischer MG, Kelly ST, Spiecker E, Steiner U, Schröder-Turk GE. 2017 Butterfly gyroid nanostructures as a time-frozen glimpse of intracellular membrane development. *Sci. Adv.* **3**, e1603119. (doi:10.1126/sciadv.1603119)
7. Saranathan V, Narayanan S, Sandy A, Dufresne ER, Prum RO. 2021 Evolution of single gyroid photonic crystals in bird feathers. *Proc. Natl Acad. Sci. USA* **118**, e2101357118. (doi:10.1073/pnas.2101357118)
8. Schoen A. 1970 Infinite periodic minimal surfaces without self-intersections. Technical Note s2-43, NASA TN D–5541.
9. Schwarz H. 1933 *Gesammelte mathematische abhandlungen*. Berlin: Springer.
10. Han L, Che S. 2018 An overview of materials with triply periodic minimal surfaces and related geometry: from biological structures to self-assembled systems. *Adv. Mater.* **30**, 1705708. (doi:10.1002/adma.201705708)
11. Park H, Jo S, Kang B, Hur K, Oh S, Ryu D, Lee S. 2022 Block copolymer gyroids for nanophotonics: significance of lattice transformations. *Nanophotonics* **11**, 2583–2615. (doi:10.1515/nanoph-2021-0644)

12. Peng W, Sun K, Onck P. 2022 Structure–property relations of three-dimensional nanoporous template-based graphene foams. *Extr. Mech. Lett.* **54**, 101737. (doi:10.1016/j.eml.2022.101737)
13. Miller DC, Terrones M, Terrones H. 2016 Mechanical properties of hypothetical graphene foams: giant Schwarzites. *Carbon* **96**, 1191–1199. (doi:10.1016/j.carbon.2015.10.040)
14. Thomson W. 1887 On the division of space with minimum partitional area. *Lond. Edinb. Dublin Phil. Mag. J. Sci.* **24**, 503–514. (doi:10.1080/14786448708628135)
15. Shan W, Thomas EL. 2024 Gradient transformation of the double gyroid to the double diamond in soft matter. *ACS Nano* **18**, 9443–9450. (doi:10.1021/acsnano.3c11101)
16. Dimitriyev M, Freenvall B, Mathew R, Grason G. 2025 Not even metastable: cubic double-diamond in diblock copolymer melts. *ACS Macro Lett.* **14**, 1291–1298. (doi:10.1021/acsmacrolett.5c00443)
17. Bonnet O. 1853 Deuxiéme note sur les surfaces a lignes de courbure sphériques. *C. R. Acad. Sci. Paris* **36**, 389–391, 585–587.
18. Fogden A, Hyde S. 1999 Continuous transformations of cubic minimal surfaces. *Eur. Phys. J. B* **7**, 91–104. (doi:10.1007/s100510050592)
19. José RG. 2024 *Modelo matemático tridimensional uniforme del Nautilus*. Cordoba: RED Descartes.
20. Theis S, Mendieta-Serrano MA, Chapa-y-Lazo B, Chen J, Saunders TE. 2025 CellMet: extracting 3D shape and topology metrics from confluent cells within tissues. *PLoS Comput. Biol.* **21**, 1–18. (doi:10.1371/journal.pcbi.1013260)
21. Yuval M, Peleg A, Ceyhan E, Tchernov D, Loya Y, Bar-Massada A, Treibitz T. 2025 Intratentacular budding and zooid-dynamics in two coral genera. *Ecol. Inf.* **90**, 103293. (doi:10.1016/j.ecoinf.2025.103293)
22. Gabbard J, van Rees WM. 2025 A high-order immersed finite-difference discretization for solving linear and nonlinear elasticity problems. *Comput. Methods Appl. Mech. Eng.* **446**, 118269. (doi:10.1016/j.cma.2025.118269)
23. Ceperic V. 2026 Soft-cell tessellations for finite element mesh generation: convergence and accuracy analysis. *Mathematics* **14**, 759. (doi:10.3390/math14050759)
24. Zhu Y, Charkieh AS, Coster AD, Pyl L. 2025 A novel hybrid intersecting spherical shell mechanical metamaterial. *Compos. Struct.* **370**, 119359. (doi:10.1016/j.compstruct.2025.119359)
25. Hosseini N *et al.* 2025 From waste to resource: transforming eggshells into modular bio-building systems. In *CAADRIA 2025: architectural informatics, Tokyo, Japan*, pp. 487–496. (doi:10.52842/conf.caadria.2025.3.487)
26. Budd G. 2021 Morphospace. *Curr. Biol.* **31**, R1141–R1224. (doi:10.1016/j.cub.2021.09.029)
27. Aroyo MI (ed.). 2016 *International tables for crystallography, volume A: space-group symmetry*. International Union of Crystallography. (doi:10.1107/97809553602060000114)
28. Mackay AL. 2015 Periodic minimal surfaces. *Nature* **314**, 604–606. (doi:10.1038/314604a0)
29. Riemann B. 1867 Über die Flche vom kleinsten Inhalt bei gegebener Begrenzung. *Abh. Königl. Ges. Wiss. Göttingen* **13**, 3–52.
30. Gandy P, Klinowski J. 2000 Exact computation of the triply periodic Schwarz P minimal surface. *Chem. Phys. Lett.* **322**, 579–586. (doi:10.1016/S0009-2614(00)00453-X)
31. Coxeter H. 1936 Regular skew polyhedra in three and four dimensions and their analogues. *Proc. Lond. Math. Soc.* **2**, 33–62. (doi:10.1112/plms/s2-43.1.33)
32. Plateau J. 1873 *Statique expérimentale et théorique des liquides soumis aux seules forces moléculaires*. Paris: Gauthier-Vilars.
33. Gong L, Kyriakides S, Triantafyllidis N. 2005 On the stability of Kelvin cell foams under compressive loads. *J. Mech. Phys. Solids* **53**, 771–794. (doi:10.1016/j.jmps.2004.10.007)
34. Weaire D. 2007 Kelvin's foam structure: a commentary. *Phil. Mag. Lett.* **88**, 91–102. (doi:10.1080/09500830701697498)
35. Bitsche R. 2005 Space-filling polyhedra as mechanical models for solidified dry foams. Master's thesis, Technical University of Vienna.
36. Daxner T, Bitsche R, Böhm H. 2006 Space-filling polyhedra as mechanical models for solidified dry foams. *Mater. Trans.* **47**, 2213–2218. (doi:10.2320/matertrans.47.2213)
37. Horváth AG. 1996 On the Dirichlet—Voronoi cell of unimodular lattices. *Geom. Dedicata* **63**, 183–191. (doi:10.1007/BF00148218)
38. Voronoi G. 1909 Nouvelles applications des paramétres continus à la théorie des formes quadratiques II. *Geom. Dedicata* **136**, 67–181. (doi:10.1515/crll.1909.136.67)